Bone Reports 12 (2020) 100276

Contents lists available at ScienceDirect

Bone Reports

journal homepage: www.elsevier.com/locate/bonr

Case Report

Lessons learnt from delayed diagnosis of FGF-23-producing tumour-induced osteomalacia and post-operative hungry bone syndrome

S. Kumar[a,*], T. Diamond[b]

[a] Basic Physician Trainee, Northern Sydney Coastal Network, Sydney, Australia
[b] St George Public Hospital, Kogarah, NSW 2217, Australia

ARTICLE INFO

Keywords:
FGF-23
Tumour-induced osteomalacia
Hypophosphataemic osteomalacia
Hypophosphataemia
Osteomalacia
Hungry bone syndrome
Bone

ABSTRACT

Tumour-induced osteomalacia (TIO) is a rare paraneoplastic syndrome caused by a fibroblast growth-factor-23 (FGF-23)-secreting phosphaturic mesenchymal tumour (PMT) and is characterised by hypophosphataemic osteomalacia. We present a 36-year-old man initially presenting with diffuse bone and joint pain who was inappropriately treated for presumed ankylosing spondylitis for 2 years. Whole-body bone scan suggested metabolic bone disease, prompting referral to our endocrine institution. He was subsequently diagnosed with persistent hypophosphataemia, inappropriately high renal tubular phosphate excretion, 1,25-dihydroxyvitamin D_3 suppression, severe osteoporosis and severe osteomalacia. FGF-23 concentrations (140 ng/L) were raised 3-fold above the upper limit of normal. Initial Gallium-68 (^{68}Ga) DOTATATE positron emission tomography (PET)/CT scan missed an active lesion in the left fibular head as the field only included the mid-brain to the proximal femora. Histopathology results from tumour resection confirmed a PMT over-expressing FGF-23. Serum phosphate and FGF-23 normalised immediately post-operatively. He developed severe hypocalcaemia 3-weeks post-operatively (1.77 mmol/L) which normalised after 1 month of high-dose caltrate and calcitriol therapy. Osteomalacia, osteoporosis and associated symptoms resolved during medium-term follow-up with > 100% improvement in his bone mineral density. This case report and discussion highlights the pitfalls contributing to delayed diagnosis of TIO and alerts clinicians to the potential complication of hungry bone syndrome post-tumour resection.

1. Introduction

Tumour-induced osteomalacia (TIO) is a rare paraneoplastic syndrome predominantly caused by a fibroblast-growth-factor-23 (FGF-23)-secreting phosphaturic mesenchymal tumour (PMT) (Folpe et al., 2004; Minisola et al., 2017). TIO is characterised by hypophosphataemic osteomalacia, impaired renal proximal tubular phosphate reabsorption, suppressed 1,25-dihydroxy-vitamin D synthesis, and elevated circulating FGF-23 concentrations (Minisola et al., 2017; Chong et al., 2011a). Somatostatin receptor (SSTR)-based functional imaging provides the highest sensitivity and specificity in locating these occult neuroendocrine tumours (Minisola et al., 2017; Zhang et al., 2015). Complete tumour resection is the only established definitive cure (Minisola et al., 2017). However, patients with TIO often suffer several years with progressive, debilitating symptoms before definitive treatment is achieved (Minisola et al., 2017; Ledford et al., 2013). Contributing factors include delayed investigation of hypophosphataemia, misdiagnosis or inability to recognise TIO as the cause for symptoms, and difficulty in locating the culprit tumour (Minisola et al., 2017; Ledford et al., 2013).

Hungry bone syndrome (HBS) is a phenomenon that occurs after parathyroidectomy in some patients with severe hyperparathyroidism (Witteveen et al., 2013; Jain and Reilly, 2017). Accelerated influx of circulating calcium and phosphate into bone to facilitate rapid remineralisation and bone formation results in severe and prolonged post-operative hypocalcaemia with or without hypophosphataemia (Witteveen et al., 2013; Jain and Reilly, 2017; Rendina et al., 2009). Treatment involves high-dose calcium and vitamin D supplementation (Witteveen et al., 2013; Jain and Reilly, 2017). HBS has very rarely been reported in patients with TIO post-tumour resection (Rendina et al., 2009).

We present a case of a 36-year-old man with hypophosphataemic osteomalacia who underwent successful surgical resection of an FGF-23-producing left fibular tumour. He had a 2-year delay from onset of symptoms to curative treatment largely due to initial incorrect diagnosis of ankylosing spondylitis, failure to investigate

* Corresponding author at: Royal North Shore Hospital, Reserve Rd, St Leonards, NSW, 2065, Australia.
E-mail address: shejil_kumar@hotmail.com (S. Kumar).

https://doi.org/10.1016/j.bonr.2020.100276
Received 26 March 2019; Received in revised form 4 April 2020; Accepted 1 May 2020
Available online 06 May 2020

hypophosphataemia and inability to recognise the syndrome of TIO. His post-operative course was complicated by HBS-induced hypocalcaemia.

2. Case presentation

A 36-year-old man initially presented to a tertiary hospital with progressively worsening pain and stiffness in his lower back, knees, shoulders, hips and lower ribs bilaterally. He had history of non-alcoholic fatty liver disease, elevated body mass index and dyslipidaemia. He was not taking any regular medications, worked as an accountant and was usually very fit and active.

Full blood count, C-reactive protein (1.1 mg/L) and erythrocyte sedimentation rate (6 mm/h) were within normal-range and results were negative for rheumatoid factor, anti-nuclear antibodies and HLA−B27. Whole-body ^{99m}Tc methylene disphosphonate (MDP) bone scan showed fractures in multiple ribs and the medial tibial condyles bilaterally, as well as increased uptake in both sacro-iliac, knee and hip joints, and several joints in the hands and feet. The pattern of involvement was deemed most consistent with ankylosing spondylitis and he was referred to a rheumatologist for ongoing management. However, the underlying cause of his non-traumatic fractures was not investigated further.

Over the following 2 years, he was managed with non-steroidal anti-inflammatory drugs, prednisone, anti-TNFα therapy (etanercept, adalimumab), and traditional Chinese medicines. Despite this, he suffered marked deterioration with worsening stiffness and weakness in his legs, recurrent falls and severe lower back and chest wall pain. He had extreme difficulty alighting from a chair and climbing up and down from a hospital bed. He began to require a walking frame to mobilise and was unable to continue working. Subsequent lumbar spine and pelvic X-Rays showed generalised osteopaenia and L1-L2 vertebral body wedging and endplate depression and sclerosis, indicating a 'rugger jersey spine'. Whole-body bone scan (Fig. 1A) revealed features of metabolic bone disease, including costochondral beading, multiple antero-lateral rib fractures bilaterally, proximal right femoral neck pseudofracture and increased activity in multiple joints bilaterally.

These results prompted referral to our endocrine service. On review of initial biochemistry 2 years prior, he had a low serum phosphate concentration on presentation (0.42 mmol/L) that remained persistently low, fluctuating between 0.30 and 0.43 mmol/L (Fig. 2). Comprehensive biochemistry (Table 1) revealed ongoing hypophosphataemia (0.47 mmol/L) with inappropriately high renal tubular phosphate excretion of 51.05% (normally 10–20% with normophosphataemia) (Florenzano et al., 2017). Serum corrected calcium (2.23 mmol/L), magnesium (0.82 mmol/L) and 25-hydroxyvitamin D_3 levels (57 nmol/L) were within normal limits. Serum parathyroid hormone (PTH) level was in the normal range (5.8 pmol/L) suggesting this was not contributing to his renal phosphate wasting (Fig. 3). 1,25-dihydroxyvitamin D3 level was suppressed (27 pmol/L) which could contribute to his hypophosphataemia but would not explain his renal phosphate wasting. He had elevated bone-specific alkaline phosphatase (ALP) levels (106 μg/L) and urine deoxypyridinoline (DPD)/creatinine ratio (15.8 μmol/mmol), indicating increased bone turnover (Fig. 3). Bone mineral density (BMD) measurements on dual energy X-ray absorptiometry (DEXA) scan (Table 2) demonstrated severe osteoporosis at the lumbar spine (0.68 g/cm^2, T-score −4.7) and left femoral neck (0.53 g/cm^2, T-score −4.1) but not the distal radius (0.96 g/cm^2, T-score −0.3). Computed tomography (CT)-guided bone biopsy was performed on the right iliac crest (Table 3). Analysis of a tetracycline-labelled, undecalcified section revealed hyperosteoidosis, increased osteoid thickness, reduced trabecular bone area, increased osteoclast number and tetracycline smearing, indicating severe osteomalacia.

Intact FGF-23 concentrations (140 ng/L) (Table 1) (Immutopics Inc., San Clemente, USA) were raised 3-fold above the upper limit of normal in the context of normal renal function (eGFR > 90 mL/min/m^2), raising suspicion for TIO. Lack of family history, adult age of onset, normal height and absence of skeletal deformities suggested genetic causes of raised FGF-23 were unlikely. Further history excluded previous intravenous administration of iron polymaltose or ferric carboxymaltose. Initial Gallium-68 (^{68}Ga) DOTATATE positron emission tomography (PET)/CT scan (Fig. 1B) including the standard field from mid-brain to proximal femora showed no evidence of an underlying SSTR-expressing tumour. However, a few days after, a repeat ^{68}Ga DOTATATE PET/CT scan (Fig. 1C–E) of the whole body (from vertex to feet) revealed focally increased tracer uptake (SUV_{max} 38.3) in the proximal end of the left fibula. Corresponding low-dose non-contrast CT scan (Fig. 1F) showed diffuse sclerosis in the posterior aspect of the proximal left fibula. Magnetic resonance imaging (MRI) scan (Fig. 4)

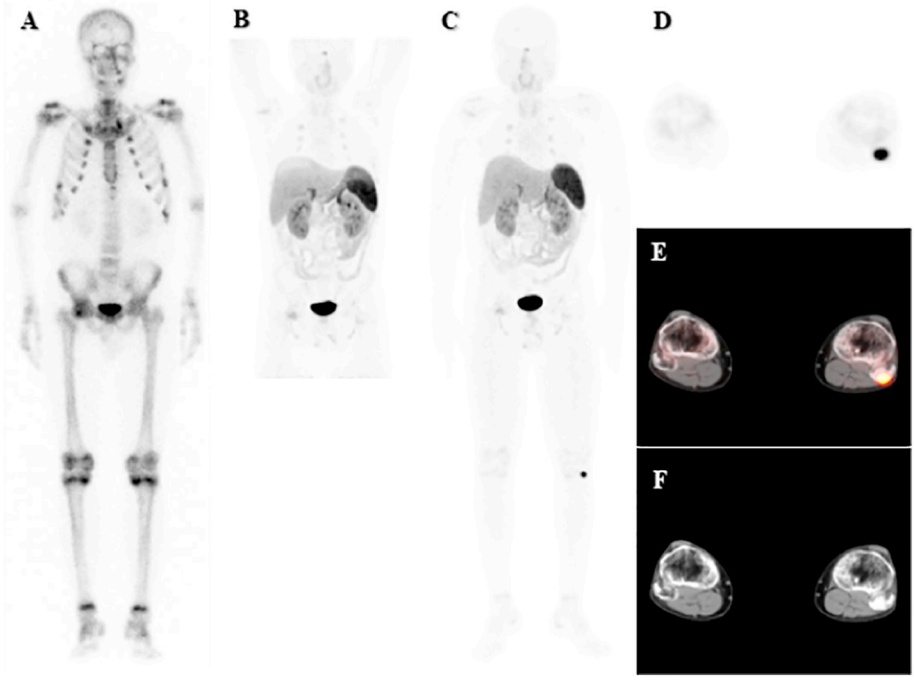

Fig. 1. ^{99m}Tc-MDP bone scintigraphy and ^{68}Ga-DOTATATE PET/CT scans

^{99m}Tc-MDP bone scan (A) demonstrated features of osteomalacia including costochondral beading, increased activity in multiple joints bilaterally (hands, shoulders, sacro-iliac, hips, knees, ankles), pseudofracture in right proximal femoral neck and stress fractures in multiple ribs bilaterally.

Initial ^{68}Ga-DOTATATE-PET/CT scan (B) missed the left fibular tumour as it only included the midbrain to proximal femora in the standard oncological field. Repeat ^{68}Ga-DOTATATE-PET/CT scan (C) highlighted a small area of intensely increased tracer uptake (SUV_{max} 38.3) just below the left knee, which did not correspond to focal abnormal activity on the bone scan.

On axial-view images of PET (D) and PET/CT fusion (E), the increased activity was localised to the proximal end of the left fibula, where diffuse sclerosis could be seen on the low-dose CT scan (F).

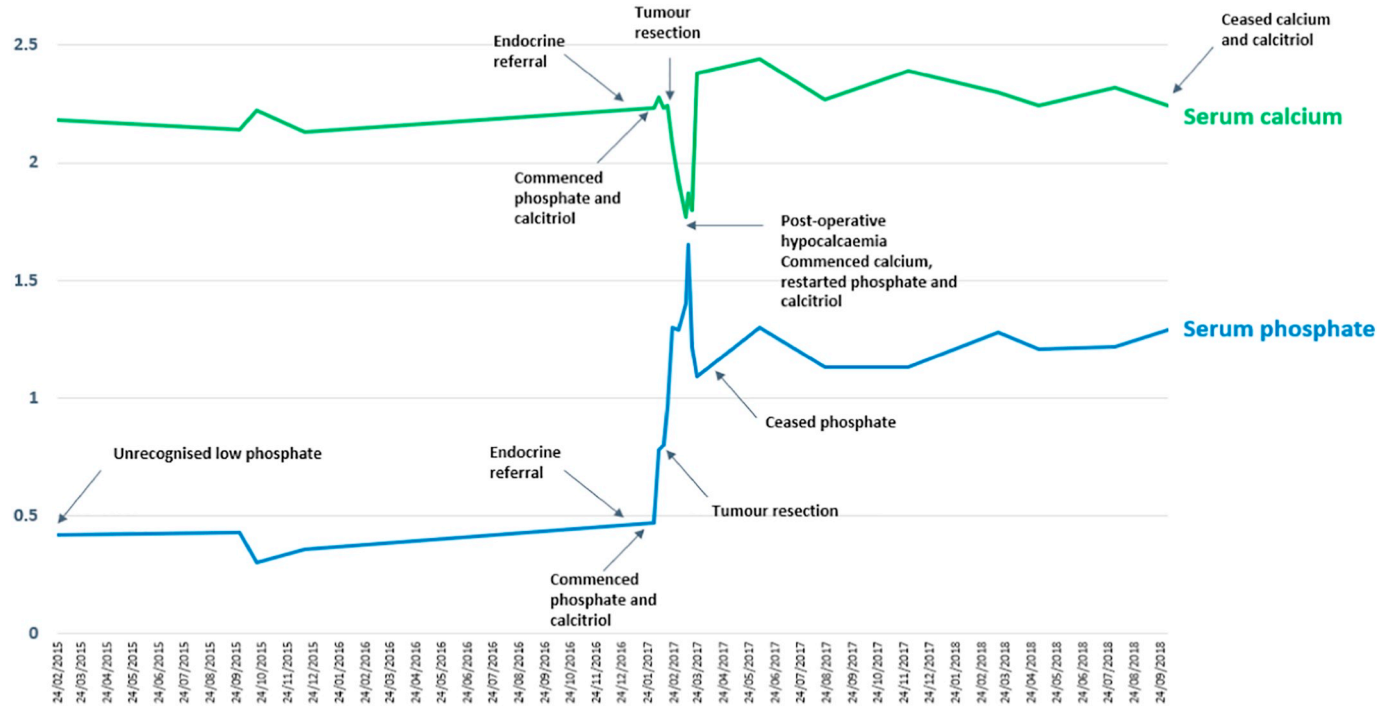

Fig. 2. Pre-operative and post-operative trends in serum calcium and phosphate concentrations
This graph demonstrates the trends over time of his serum calcium and phosphate concentrations from his initial presentation 2 years pre-tumour resection (far-left) to 1.5 years post-tumour resection (far-right). He had persistent hypophosphataemia before recognition. Phosphate and calcitriol was commenced 2 weeks pre-operatively, shortly after endocrine referral. Within 2 days post-operatively, serum phosphate normalised after swhich phosphate and calcitriol supplementation was ceased. Three weeks post-operatively, he developed severe hypocalcaemia to 1.77 mmol/L prompting high-dose caltrate (1200 mg QID) and calcitriol (0.5 μg QID) and phosphate which normalised calcium concentration and maintained normal serum phosphate concentration after 1 month, at which point phosphate was ceased. Over the following 1.5 years, his calcium and calcitriol therapy was slowly de-escalated and ceased after repeat bone biopsy confirmed resolution of osteomalacia.

Table 1
Pre-operative results of phosphate, calcium and bone-related biochemistry.

Study	Interpretation	Pre-operative result	Normal range (units)
Serum phosphate	Low	0.47	0.8–1.5 (mmol/L)
Renal tubular phosphate excretion	High	51.05	85–95 (%)
Serum corrected calcium	Normal	2.23	2.15–2.55 (mmol/L)
Serum magnesium	Normal	0.82	0.70–1.10 (mmol/L)
Serum PTH	Normal	5.8	1.6–6.9 (pmol/L)
Serum 25-hydroxy-vitD_3	Normal	57	50–140 (nmol/L)
Serum 1–25-dihydroxy-vitD_3	Low	27	60–210 (pmol/L)
Serum bone-specific ALP	High	106	5.5–24.6 (μg/L)
Urine DPD/creatinine ratio	High	15.8	2.3–5.4 (μmol/mmol)
Serum intact FGF-23	High	140	10–54 (ng/L)

PTH = parathyroid hormone; vitD3 = vitamin D3; ALP = alkaline phosphatase; DPD = deoxypyridinoline; FGF-23 = fibroblast growth factor-23
Pre-operative results highlight consequences of elevated circulating FGF-23 levels: serum hypophosphataemia due to excess renal tubular phosphate excretion and suppressed 1-25-dihydroxy-vitD_3, with associated accelerated bone turnover (elevated bone-specific ALP and urine DPD/creatinine ratio). Hypomagnasaemia and hyperparathyroidism were excluded as causes of hypophosphataemia.

confirmed a well-marginated 17–18 mm lesion in the left fibular head demonstrating diffuse contrast enhancement, T1-weighted hypointensity and T2-weighted hyperintensity.

Two weeks prior to tumour resection, he was commenced on high-dose phosphate (1000 mg TDS) and calcitriol (0.5 μg TDS). He then underwent en-bloc tumour resection. An astronomically high intact FGF-23 concentration found in the ex-vivo tumour aspiration (16,600 ng/L) confirmed the left fibular tumour as the ectopic source of excess circulating FGF-23. Histopathological examination (Fig. 5) demonstrated complete resection of an entirely intraosseous tumour classified as PMT-mixed connective tissue variant (PMT-MCT), with clean resection margins. Tumour tissue consisted of proliferation of bland elongated spindle and stellate cells with well-developed vasculature, occasional areas of hyper-cellularity and nuclear atypica, and the absence of frequent mitoses and necrosis. Immunohistochemistry showed diffuse strongly positive staining for FGF-23 and SSTR2A.

Within 2 days post-operatively, serum intact FGF-23 was undetectable and serum phosphate concentrations normalised (0.96 mmol/L) (Fig. 2). Phosphate and calcitriol therapy were subsequently ceased. Three weeks post-operatively, he developed muscle cramps associated with profound hypocalcaemia to 1.77 mmol/L (Fig. 2) and compensatory decrease in urinary calcium excretion to 0.7 mmol/day, suggestive of HBS. Serum phosphate and magnesium concentrations were normal. He was treated with high-dose caltrate (1200 mg QID) and calcitriol (0.5 μg QID) to restore circulating calcium deficit. Phosphate supplementation was also recommenced (500 mg BD) to help maintain normophosphataemia. His serum calcium (2.38 mmol/L) and urinary calcium excretion (5.8 mmol/day)

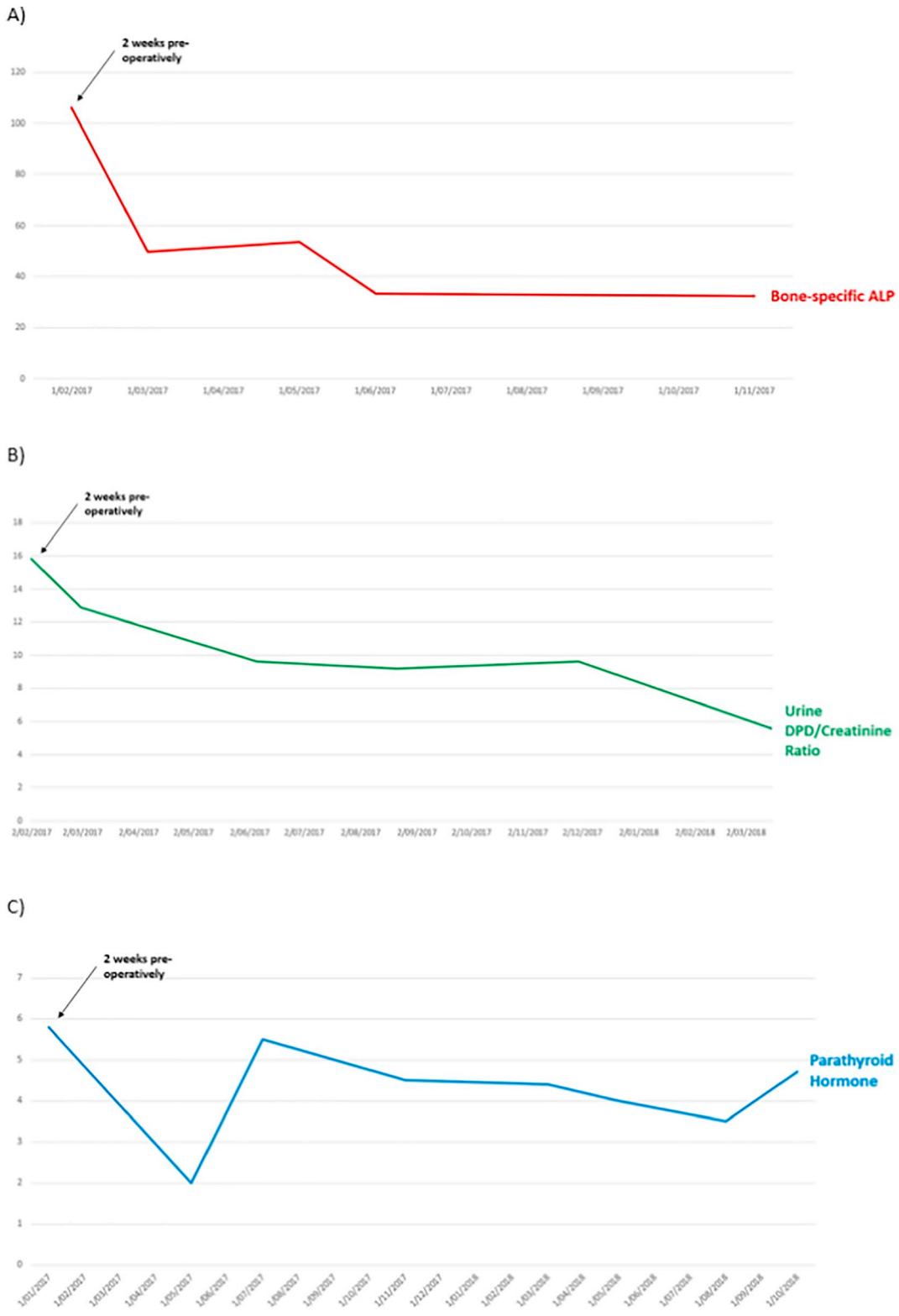

Fig. 3. Pre-operative levels and post-operative trends in bone turnover markers and PTH
PTH = Parathyroid hormone; ALP = Alkaline phosphatase; DPD = deoxypyridinoline
This graph demonstrates increased levels of bone turnover markers, bone-specific ALP (normal range 3.7–20.9 μg/L) and urine DPD/creatinine ratio (normal range 2.3–5.4 μmol/mmol), 2 weeks pre-operatively and their subsequent decline post-operatively. However both markers remained elevated at approximately 1-year post-operatively. Serum PTH remained within the normal range (1.5–9.9 pmol/L) throughout his course.

subsequently normalised after 1 month, while serum phosphate remained within the normal range, at which point phosphate was ceased. Therapy was de-escalated to 1200 mg BD caltrate and 0.25 μg BD calcitriol shortly afterwards. Thoracolumbar spinal X-rays 2 months post-resection demonstrated significant new bone formation and osteosclerosis at the vertebral end plates (Fig. 6). Bone-specific ALP and urine DPD/creatinine ratio gradually decreased over the following months (Fig. 3). Repeat DEXA studies 6 months post-resection (Table 2)

Table 2
Comparison between pre- and post-operative BMD results based on DEXA imaging.

DEXA study	Pre-operative result	Post-operative result (6 months)	Improvement from baseline	Post-operative result (18 months)	Improvement from baseline
Lumbar spine BMD	0.677 g/cm^2	1.323 g/cm^2	+0.646 g/cm^2 (95.4%)	1.293 g/cm^2	+0.616 g/cm^2 (91.0%)
Lumbar spine T-score	−4.7	−0.5	–	+0.4	–
Lumbar spine result	Severe osteoporosis	Normal	–	Normal	–
Left femoral neck BMD	0.531 g/cm^2	1.008 g/cm^2	+0.477 g/cm^2 (89.8%)	1.260 g/cm^2	+0.729 g/cm^2 (137.3%)
Left femoral neck T-score	−4.1	+0.7	–	+1.5	–
Left femoral neck result	Severe osteoporosis	Normal	–	Normal	–
Distal radius BMD	0.958 g/cm^2	0.977 g/cm^2	+0.019 g/cm^2 (1.8%)	0.962 g/cm^2	+0.004 g/cm^2 (0.4%)
Distal radius T-score	−0.3	−0.1	–	−0.3	–
Distal radius result	Normal	Normal	–	Normal	–

Lumbar spine = L2-L4; DEXA = dual-energy X-ray absorptiometry; BMD = bone mineral density; Osteoporosis = T-score below −2.5 (> 2.5 standard deviations below the mean)
Results demonstrate severe pre-operative osteoporosis at the lumbar spine and left femoral neck with sparing of the distal radius. Post-operative DEXA BMD demonstrated resolution of severe osteoporosis and significant improvement in BMD at lumbar-spine and left femoral neck, with negligible changes seen at the distal radius. Improvements in BMD were sustained at 18-months follow-up.

Table 3
Un-decalcified iliac crest biopsy histopathology results demonstrating high bone formation/remodelling and resolution of osteomalacia at 18-months follow-up.

Parameter	Pre-operative result	Post-operative result	Normal range for men 40–60 years old
Trabecular bone area	6.9^{L}	32.4^{H}	21–29%
Cortical width	–	1.18	0.8–1.4 mm
Relative osteoid area	60.4^{H}	4.8^{H}	1.3–3.1%
Total osteoid surface	75^{H}	38.3^{H}	7.1–13.9%
Active resorption surface	1.3	1.1	0.5–2.5%
Total resorption surface	3.6	5.2	2.2–6.7%
Osteoclasts number	2.8^{H}	0.6	0.3–1.3 cells/cm^2
Double label surface	Tetracycline smearing	32.6^{H}	4.2–11.6%
Mineral appositional rate	Tetracycline smearing	1.58^{H}	0.60–0.80 mm/day
Bone formation rate	Tetracycline smearing	0.52^{H}	0.03–0.09 mm^3/mm^2/day
Osteoid seam width	36.8^{H}	26.8^{H}	9.2–14.9 μm
Mineralisation lag time	–	20.3	12.1–19.9 days
Fibrous area	0	0.5	0%
Aluminium surface	0	0	0%

H = high, L = low
Results demonstrate pre-operative reduced trabecular bone area, hyperosteoidosis, increased osteoclast number and tetracycline smearing suggestive of severe osteomalacia. At 18-months follow-up, mildly increased trabecular bone area, increased osteoid surface and thickness and increased bone formation rate with normal mineralisation lag time indicated high bone formation/remodelling and absence of osteomalacia.

showed significant improvement in BMD of 95.4% at the lumbar spine (1.32 g/cm^2, T-score +0.7) and 89.8% at the left femoral neck (1.01 g/cm^2, T-score −0.5). His therapy was subsequently de-escalated to 0.25 μg BD calcitriol and 600 mg caltrate daily. At 9 months post-operatively, serum procollagen type 1 N-terminal propeptide (P1NP), a marker of bone formation, was elevated to twice the upper limit of normal (151 ng/mL). After 1 year post-operatively, his skeletal pain and stiffness and muscle weakness had completely resolved and he had returned to his pre-morbid level of functioning and mobility and resumed his active lifestyle. At 18 months post-resection, repeat lumbar spine X-ray (Fig. 6) demonstrated healing of previous 'rugger jersey' spine. Bone-specific ALP levels remained elevated (32.3 μg/L) and improvements in BMD (Table 2) were sustained with a 137.3% increase in left femoral neck BMD from baseline. Repeat iliac crest bone biopsy (Table 3) showed persistent but reduced hyperosteoidosis and marked increase in trabecular bone area and tetracycline-labelled bone formation and normal mineralisation lag time, confirming resolution of osteomalacia. His calcium and vitamin D therapy was thereafter ceased.

3. Case discussion

The causative tumours in TIO are predominantly benign and overexpress FGF-23 (Folpe et al., 2004; Minisola et al., 2017). FGF-23 is physiologically released by osteoblasts and osteocytes and acts to decrease serum phosphate concentrations through two mechanisms (Florenzano et al., 2017; Bergwitz and Juppner, 2010; Bhattacharyya et al., 2012). Firstly, FGF-23 reduces expression of sodium-phosphate co-transporters 2a and 2c at the apical membrane of the renal proximal tubule and thus inhibits renal tubular phosphate reabsorption and promotes renal phosphate excretion (Florenzano et al., 2017; Bergwitz and Juppner, 2010; Bhattacharyya et al., 2012). Secondly, FGF-23 inhibits expression of renal 1-α-hydroxylase and thus reduces synthesis of active vitamin D and indirectly, gastrointestinal phosphate absorption (Florenzano et al., 2017; Bergwitz and Juppner, 2010; Bhattacharyya et al., 2012). Therefore, excess circulating FGF-23 in TIO results in renal phosphate wasting and active vitamin D deficiency, culminating in the hypophosphataemia seen in our patient (Florenzano et al., 2017; Boland et al., 2018). His chronic hypophosphataemia caused osteomalacia, osteoporosis, multiple stress fractures, diffuse bone pain and muscle weakness (Minisola et al., 2017; Boland et al., 2018). The extraordinarily high FGF-23 levels in tumour aspiration, diffusely strong expression of FGF-23 on immunohistochemistry and rapid decline in serum FGF-23 concentrations after complete tumour resection confirmed the tumour as the ectopic source of excess circulating FGF-23. Our patient was commenced on appropriate phosphate and calcitriol therapy. Prior to tumour resection or if surgery is not feasible, high-dose phosphate (1–3 g/day) divided into 4–6 doses to minimise gastrointestinal upset, and calcitriol (starting at 1.5 μg/day) is recommended to improve symptoms and begin healing of osteomalacia (Florenzano et al., 2017). Phosphate should not be commenced alone as this can promote secondary hyperparathyroidism (Florenzano et al., 2017; Boland et al., 2018). The resolution of hypophosphataemic

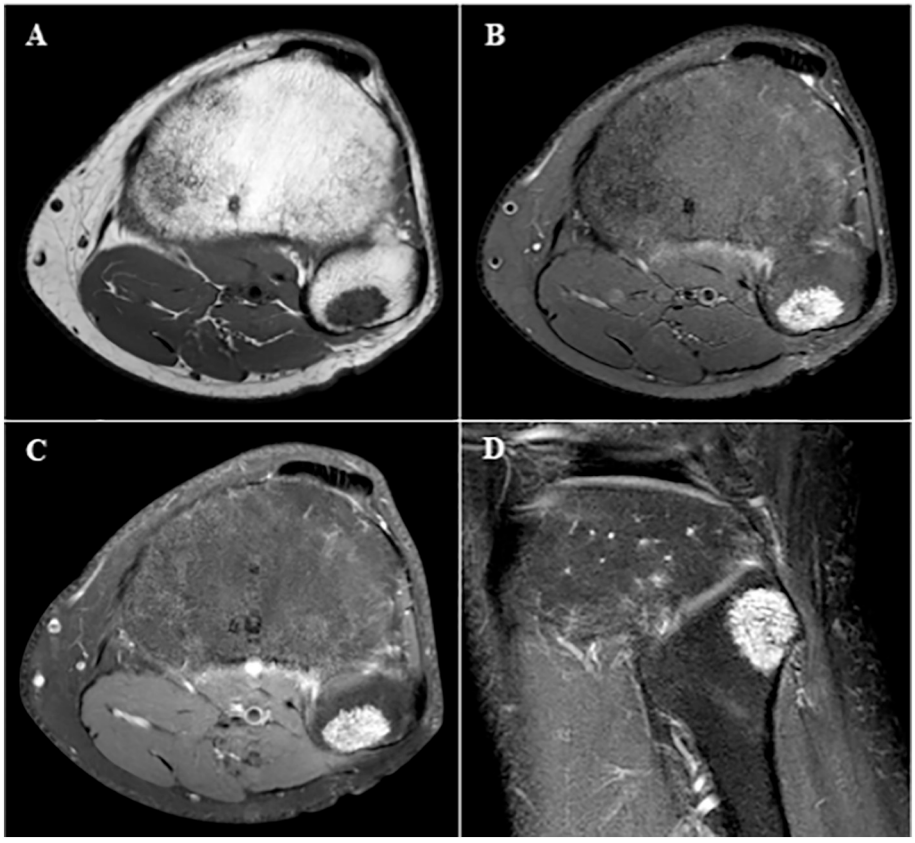

Fig. 4. Pre-operative left fibular MRI scan
Pre-operative MRI scan of the left fibula confirmed a well-marginated 17–18 mm lesion located entirely within the left fibular head. The tumour demonstrated T1-weighted hypointensity (A) and T2-weighted hyperintensity (B) on axial-view images, and prominent diffuse contrast enhancement on axial- (C) and coronal-view (D) images.

osteomalacia within months of complete tumour resection established that the FGF-23-producing tumour was the cause of the patient's morbidity.

Despite the successful outcome, our patient suffered progressively debilitating symptoms for 2 years before definitive treatment, to the extent that a previously healthy and active 36-year-old man required a walking frame to ambulate and was unable to continue working. Patients with TIO often experience several years of delay between symptom onset and curative treatment, historically ranging between 2 and 28 years (Minisola et al., 2017). Most recently, a retrospective analysis of 197 patients diagnosed with TIO in China from 2008 to 2017 discovered a mean duration of 5.7 years between symptom onset and tumour resection (Li et al., 2018). Delayed recognition or appreciation of serum hypophosphataemia is a potential contributing factor (Halperin et al., 2007; Lewiecki et al., 2008). Our patient had hypophosphataemia to 0.42 mmol/L when he initially presented to a tertiary hospital, and persistent hypophosphataemia for a further 2 years without recognition until he was referred to our endocrine service. In the same Chinese analysis, 43.1% of patients with TIO initially had hypophosphataemia missed and only 11.8% had phosphate levels checked on initial presentation (Li et al., 2018). Hypophosphataemia is a highly sensitive marker for TIO and occurs in virtually all patients (Zhang et al., 2015; Li et al., 2018; Sun et al., 2015; Jiang et al., 2012), although is non-specific and can be the result of several genetic (Chong et al., 2011a; Lewiecki et al., 2008) (e.g. X-linked or autosomal hypophosphataemic osteomalacia) or acquired causes (Chong et al., 2011a; Florenzano et al., 2017; Boland et al., 2018) (e.g. vitamin D deficiency, hyperparathyroidism, Fanconi syndrome). More prompt investigation for causes of his hypophosphataemia and multiple stress fractures could have led to an earlier diagnosis of TIO.

Another common reason for delayed diagnosis is initial misdiagnosis or the inability to recognise TIO as the cause of symptoms (Minisola et al., 2017). The symptoms reported by patients with a PMT are diffuse and non-specific, such as widespread bone and joint pain and diffuse weakness, and relate to the paraneoplastic syndrome of hypophosphataemic osteomalacia (Minisola et al., 2017). The tumours themselves are classically small, benign and slow-growing and thus any local pain that could clinically indicate the tumour's location is usually masked (Minisola et al., 2017; Zhang et al., 2015). For example, our patient did not particularly complain of pain below his left knee more so than in other painful areas of his body. Further, due to the non-specific symptoms, cases can often be misdiagnosed as inflammatory polyarthritis, musculoskeletal disorders, or even psychiatric disorders (Minisola et al., 2017; Chong et al., 2011a; Ledford et al., 2013; Halperin et al., 2007; Lewiecki et al., 2008; van der Rest et al., 2011; Teasell and Shapiro, 2002; Leow et al., 2014). Our patient was incorrectly diagnosed with ankylosing spondylitis given generalised joint pain and stiffness and increased activity in several joints bilaterally on the initial bone scan. He received inappropriate, ineffective treatment for 2 years, including prednisone which could have worsened his osteoporosis. Greater awareness is needed for the potential diagnosis of TIO in patients with persistent hypophosphataemia, progressive widespread skeletal pain, stress fractures and muscle weakness (Chong et al., 2011a; Florenzano et al., 2017).

Once symptoms are attributed to TIO, localisation of the tumour presents a major challenge (Minisola et al., 2017; Florenzano et al., 2017), and is crucial given surgical resection is the only established definitive cure (Minisola et al., 2017; Florenzano et al., 2017). Localisation of causative tumours has seen significant advancement in recent years with the development of SSTR-based functional imaging (Minisola et al., 2017; Hofman et al., 2015). ^{68}Ga-DOTATATE PET/CT scans selectively identify SSTR2-avid tissue (Reubi et al., 2000; Shastry et al., 2010) and thus are well-designed to detect PMTs, which usually express SSTR2A (Houang et al., 2013; Agaimy et al., 2017). The somatostatin analogue tyrosine-3-octreotate (TATE) is linked to a positron emitter (Gallium-68) with DOTA as the linking agent (Hofman et al., 2015). This ^{68}Ga-DOTA-TATE conjugate is intravenously administered (Hofman et al., 2015) and forms a complex with SSTR2, internalising

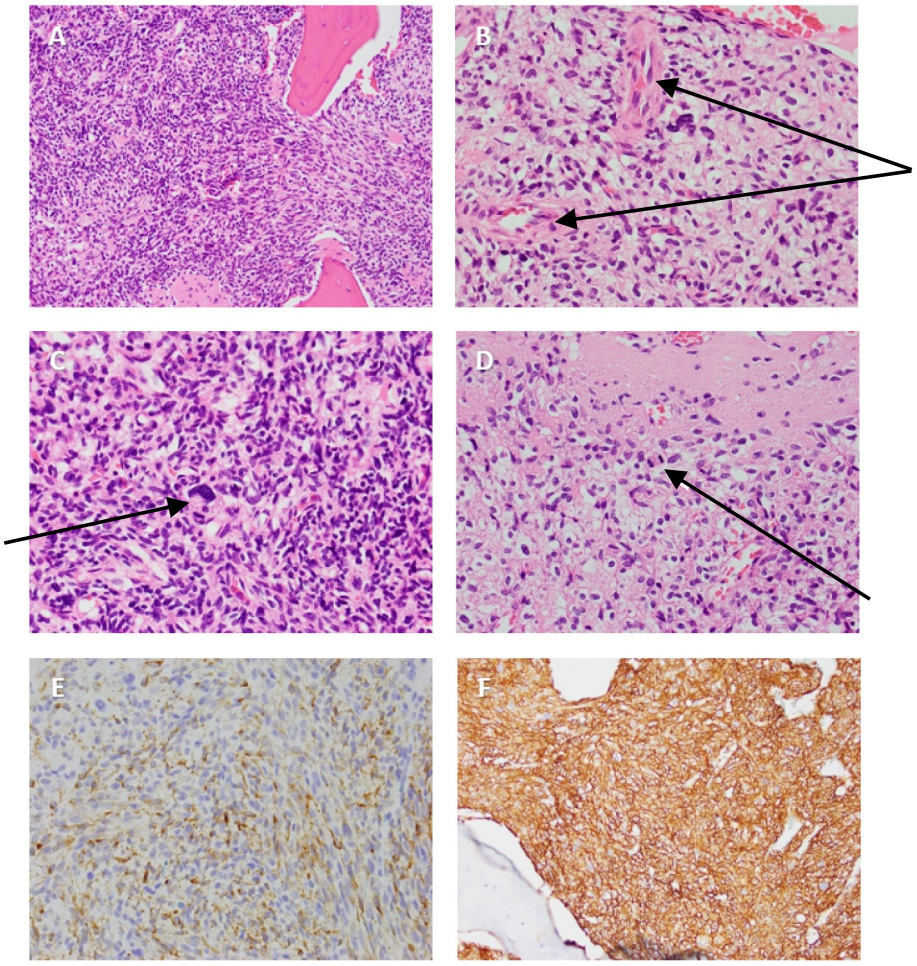

Fig. 5. Histopathological examination of left fibular tumour confirming phosphaturic mesenchymal tumour
Histopathology (obtained from complete tumour resection) with hematoxylin and eosin staining showing proliferation of bland elongated spindle and stellate cells (A) with well-developed vasculature (B), occasional areas of nuclear atypia with pleomorphism (C) and rare mitoses (D). Diffusely strong positive staining for FGF-23 (E) and SSTR2A (F) are also shown. Images provided courtesy of Dr. Fiona Bonar, histopathologist at Douglas Hanly Moir Pathology, Sydney, NSW, Australia.

into SSTR2-avid tissue (Cescato et al., 2006). The radioactive decay emitted by ^{68}Ga is detected by PET, with CT providing more precise anatomical characterisation (Hofman et al., 2015). By this method, our patient's neuroendocrine tumour, which showed diffusely strong SSTR2A expression, also displayed markedly increased activity (SUV_{max} 38.3) on the DOTATATE scan and was localised to the left fibular head. Although studies have been limited by small sample size, the DOTATATE scan has demonstrated high sensitivity and specificity in detecting PMTs (Table 4) (Zhang et al., 2015; Ho, 2015; Clifton-Bligh et al., 2013; Breer et al., 2014; Jadhav et al., 2014; Agrawal et al., 2015; El-Maouche et al., 2016) and superiority over other somatostatin receptor-based studies and the fluorodeoxyglucose (FDG)-PET/CT scan (Breer et al., 2014; Jadhav et al., 2014; Agrawal et al., 2015; El-Maouche et al., 2016). DOTATATE PET/CT scans are replacing Octreotide SPECT/CT scans in this context due to certain advantages including better spatial resolution, higher affinity for SSTR2, greater accuracy, shorter scanning time, less radiation exposure and more precise anatomic localisation (Hofman et al., 2015; Rayamajhi et al., 2019). PMTs predominantly occur in bone (40%) or soft tissue (55%) (Jiang et al., 2012) anywhere from head to toe (Folpe et al., 2004; Minisola et al., 2017; Chong et al., 2011a), but are most commonly located in the lower limbs (40–55%) (Zhang et al., 2015; Li et al., 2018; Jiang et al., 2012). Therefore, several authors have stressed the importance of scanning the entire body from head-to-toe including the extremities which are routinely not included in the standard oncological field (Minisola et al., 2017; Chong et al., 2011a; Chong et al., 2011b). Our patient's case demonstrates the potential dangers of avoiding whole-body scanning as his initial DOTATATE scan was unable to detect the left fibular tumour as the study field failed to include his distal lower limbs. Had this not been rectified shortly afterwards with a whole-body DOTATATE scan, he could have suffered a considerably longer delay until curative surgical resection.

Bone scintigraphy, on the other hand, has limited utility in locating causative tumours in patients with TIO (Minisola et al., 2017; Lee et al., 1995; Garcia and Spencer, 2002; Sood et al., 2013). The largest related study-to-date retrospectively analysed 91 patients with confirmed TIO to determine whether their tumours were identifiable on bone scans performed prior to tumour localisation by other means (Wang et al., 2018). In 77% of patients (70/91), tumour location did not correspond to increased activity on the bone scan, whereas in 23% of patients (21/91), focally increased activity was seen in the region of the tumour (Wang et al., 2018). However, even with the benefit of hindsight, our patient's bone scan did not demonstrate focally increased uptake below the left knee. Despite this, the utility of bone scans in patients with TIO can be extended to their ability to demonstrate features of widespread osteomalacia (Sood et al., 2013). Thus, bone scans, which are usually the first imaging study performed in these patients due to their diffuse bone pain, can assist clinicians in arriving at the diagnosis of TIO by prompting the investigation for causes of metabolic bone disease (Sood et al., 2013; Wang et al., 2018). Typical features of osteomalacia such as costochondral beading, increased activity in several sites bilaterally

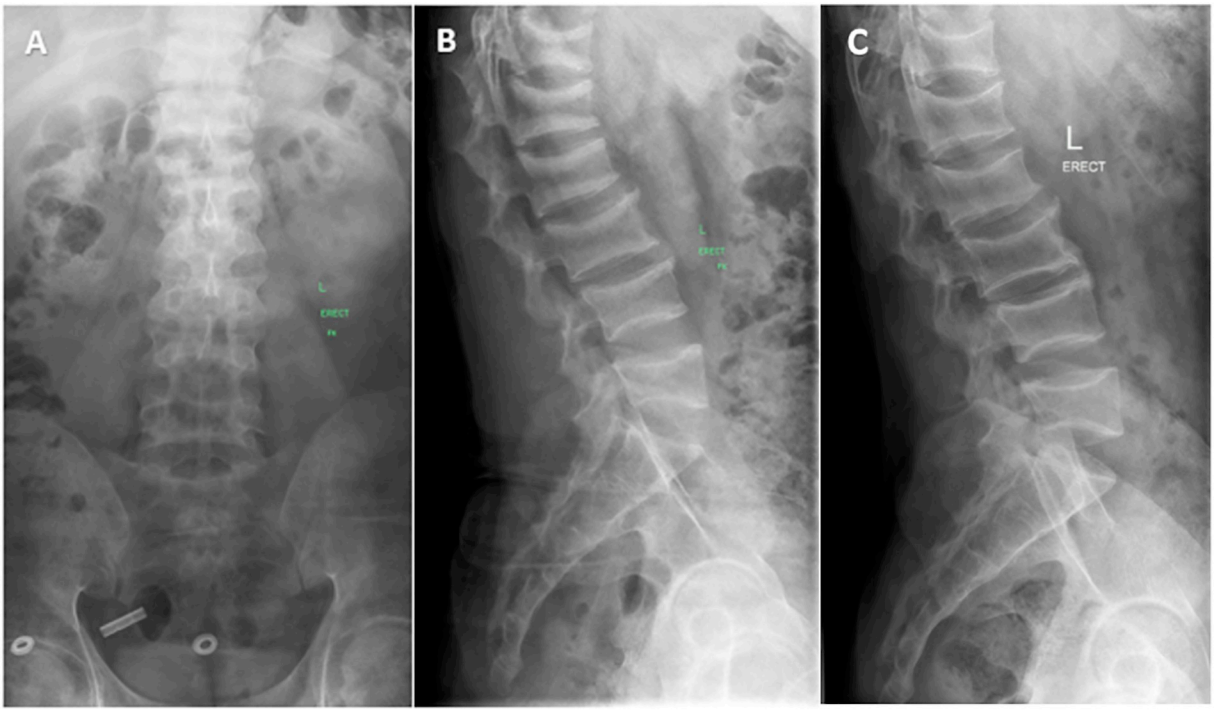

Fig. 6. Spinal X-rays demonstrating healing of 'rugger jersey spine'
Anterior-posterior (A) and lateral (B) thoracolumbar spinal X-rays 2 months post-operatively demonstrating mild kyphoscoliosis convex to the left, multiple compression fractures, significant new bone formation and significant osteosclerosis at the vertebral end plates. Repeat lumbar spine X-ray 18 months post-operatively (C) demonstrated healing of previous 'rugger jersey spine'.

Table 4
Summary of studies reporting accuracy of ^{68}Ga-DOTATATE PET/CT scan in locating the causative tumour in patients with TIO.

Authors and year of publication	Number of patients	Positive scan	Histopathologically proven	Sensitivity	Specificity
Zhang et al. (2015)	54	33	32	100%	90.9%
Ho (2015)	3	3	3	100%	–
Clifton-Bligh et al. (2013)	6	6	6	100%	–
Breer et al. (2014)	5	5	5	100%	–
Jadhav et al. (2014)	7	7	7	100%	–
Agrawal et al. (2015)	6	5	5	83.3%	100%
El-Maouche et al. (2016)	11	7	6	54.5%	85.7%

including proximal femora and wrists, and multiple stress fractures were evident in our patient's bone scan (Sood et al., 2013; Wang et al., 2018; Rai et al., 1981; Fogelman et al., 1978) and prompted referral to our endocrine service. Osteomalacia in our case was confirmed on iliac crest bone biopsy, which is not an essential investigation but has been used in patients with TIO as an adjunct to confirm osteomalacia as well as providing a baseline such that resolution of osteomalacia can be demonstrated on post-treatment biopsy. It may also be useful in differentiating osteomalacia from osteoporosis as the cause of multiple fractures.

HBS is a well-described phenomenon occurring after parathyroidectomy in patients with severe hyperparathyroidism (Witteveen et al., 2013; Jain and Reilly, 2017; Karunakaran et al., 2018), however, to our knowledge, only 3 such cases have been described after tumour resection in patients with TIO (Rendina et al., 2009). HBS post-parathyroidectomy is characterised by severe (< 2.1 mmol/L) and prolonged (> 4 days) post-operative hypocalcaemia with or without hypophosphataemia and hypomagnesaemia due to extensive accelerated mineralisation and formation of bone following the sudden decrease in PTH levels (Witteveen et al., 2013; Jain and Reilly, 2017). Treatment aims at replenishing the circulating calcium deficit and involves high-dose supplementation of calcium and active vitamin D (Witteveen et al., 2013; Jain and Reilly, 2017). The recommended daily dose for calcitriol is 2-4 μg/day and 4–12 g/day calcium, preferably calcium carbonate due to greater concentration of elemental calcium (Jain and Reilly, 2017). After tumour resection, as a result of increased phosphate availability due to rapid decline in FGF-23 concentrations, our patient's chronically unmineralized bone underwent rapid healing and active remineralisation (Florenzano et al., 2017), resulting in significant skeletal mineral uptake and depletion of circulating calcium (Witteveen et al., 2013; Jain and Reilly, 2017; Rendina et al., 2009). This was evidenced by the rapid and persistent decline in serum calcium concentrations for 1 month (despite high-dose calcium and calcitriol therapy) and compensatory reduced urinary calcium excretion at 3 weeks post-operatively. Characteristically in patients with HBS, bone-specific ALP rises in the first 1–2 months post-parathyroidectomy and can sometimes remain elevated at 12 months (Witteveen et al., 2013; Jain and Reilly, 2017; Rendina et al., 2009; Ho et al., 2017). Our patient's serum P1NP was elevated at 9 months post-operatively, and bone-specific ALP levels remained elevated at 18 months post-operatively, suggesting prolonged increased osteoblastic activity. Our patient exhibited pre-operative risk factors for HBS such as secondary hyperparathyroidism, elevated markers of bone turnover, osteoporosis and radiological evidence of metabolic bone disease (Witteveen et al., 2013; Jain and Reilly, 2017; Karunakaran et al., 2018; Kaya et al., 2016). However, there is no established preventative measure, as although pre-operative

bisphosphonate and vitamin D therapy have shown benefit, results have been conflicting and limited to case reports and small case series (Witteveen et al., 2013; Jain and Reilly, 2017). Our patient received high-dose oral calcitriol pre-operatively which did not prevent development of HBS. Burosumab, a human monoclonal antibody that neutralises FGF-23 has recently been approved in treatment of X-linked hypophosphataemic osteomalacia in children and adolescents (Lamb, 2018). In this population, burosumab has been shown to increase serum phosphate, 1,25-dihydroxyvitamin D_3 and renal tubular phosphate reabsorption, reduce osteomalacia severity and promote fracture healing without inducing hypocalcaemia (Lamb, 2018; Insogna et al., 2018). In a recent phase II trial of 8 patients with TIO, 4-weekly burosumab significantly increased serum phosphate and 1,25-dihydroxyvitamin D_3 and reduced evidence of bone turnover and severity of osteomalacia over 48 weeks (Lamb, 2018). A recent case report demonstrated improvement in serum phosphate, pain and mobility with monthly burosumab in a patient with unresectable intracranial TIO (Day et al., 2019). Burosumab is therefore a potential future therapy for patients with inoperative TIO or prior to surgical resection, and may also reduce the risk of HBS, however has not specifically been studied for this indication. Post-operatively in our patient, HBS was managed effectively with high-dose calcium and calcitriol which slowly resolved hypocalcaemia. Serum calcium, phosphate and PTH concentrations remained stable in the normal-range long-term. Further, he enjoyed the benefits of HBS (Rendina et al., 2009) with an almost 100% improvement in lumbar spine and femoral neck BMD 6 months after tumour resection and a remarkable 137.3% increase in left femoral neck BMD at 18 months post-operatively, in comparison to the expected 30.9–49.3% improvement in BMD at 6-months post-operatively (Yin et al., 2018). Although the management of our patient and interpretation of the case was limited by the failure to systematically measure calcium, phosphate and bone-related biochemistry simultaneously at regular intervals during the immediate post-operative period and during follow-up, this did not impact negatively on his overall outcome.

4. Conclusion

We have described a case of a 36-year-old man with progressively worsening skeletal pain and stiffness and muscle weakness initially diagnosed with ankylosing spondylitis. He was correctly diagnosed 2 years later with hypophosphataemic osteomalacia and osteoporosis due to renal phosphate wasting and active vitamin D deficiency, induced by an FGF-23-producing tumour located in the proximal end of his left fibula. DOTATATE scan initially missed the tumour as it did not include the distal lower limbs in the study field. Tumour resection led to rapid normalisation of serum FGF-23 and phosphate concentrations, however prolonged, severe hypocalcaemia occurred as part of a hungry bone syndrome which was successfully managed with high-dose calcium and vitamin D supplementation. In the long-term he enjoyed full recovery from debilitating symptoms, successful return to pre-morbid level of functioning, marked improvement in bone mineral density and resolution of severe osteomalacia. This case highlights several factors contributing to delayed treatment in patients with TIO including failure to investigate hypophosphataemia and stress fractures, misdiagnosis or inability to recognise TIO, and failing to utilise whole-body DOTATATE scanning to locate the causative tumour. A discussion of the features and management of his hungry bone syndrome provides insights into and raises awareness for this phenomenon which has rarely been reported in patients with TIO.

Declaration of competing interest

The authors listed above declare we have no conflicts of interest to declare in terms of the preparation or submission of this manuscript to “BONE REPORTS” for consideration for publication.

References

Agaimy, A., Michal, M., Chiosea, S., et al., 2017. Phosphaturic mesenchymal tumors: clinicopathologic, immunohistochemical and molecular analysis of 22 cases expanding their morphologic and immunophenotypic spectrum. Am. J. Surg. Pathol. 41 (10), 1371–1380.

Agrawal, K., Bhadada, S., Mittal, B.R., et al., 2015. Comparison of 18F-FDG and 68Ga DOTATATE PET/CT in localization of tumor causing oncogenic osteomalacia. Clin. Nucl. Med. 40 (1), e6–e10.

Bergwitz, C., Juppner, H., 2010. Regulation of phosphate homeostasis by PTH, vitamin D, and FGF23. Annu. Rev. Med. 61, 91–104.

Bhattacharyya, N., Chong, W.H., Gafni, R.I., et al., 2012. Fibroblast growth factor 23: state of the field and future directions. Trends Endocrinol. Metab. 23 (12), 610–618.

Boland, J.M., Tebben, P.J., Folpe, A.L., 2018. Phosphaturic mesenchymal tumors: what an endocrinologist should know. J. Endocrinol. Investig. 41 (10), 1173–1184.

Breer, S., Brunkhorst, T., Beil, F.T., et al., 2014. 68Ga DOTA-TATE PET/CT allows tumor localization in patients with tumor-induced osteomalacia but negative 111In-octreotide SPECT/CT. Bone 64, 222–227.

Cescato, R., Schulz, S., Waser, B., et al., 2006. Internalization of sst2, sst3, and sst5 receptors: effects of somatostatin agonists and antagonists. J. Nucl. Med. 47 (3), 502–511.

Chong, W.H., Molinolo, A.A., Chen, C.C., et al., 2011a. Tumor-induced osteomalacia. Endocr. Relat. Cancer 18 (3), R53–R77.

Chong, W.H., Yavuz, S., Patel, S.M., et al., 2011b. The importance of whole body imaging in tumor-induced osteomalacia. J. Clin. Endocrinol. Metab. 96 (12), 3599–3600.

Clifton-Bligh, R.J., Hofman, M.S., Duncan, E., et al., 2013. Improving diagnosis of tumor-induced osteomalacia with Gallium-68 DOTATATE PET/CT. J. Clin. Endocrinol. Metab. 98 (2), 687–694.

Day, A.L., Gutierrez, O.M., Guthrie, B.L., Saag, K.G., 2019. Burosumab in tumor-induced osteomalacia: a case report. Joint Bone Spine 30118–6.

El-Maouche, D., Sadowski, S.M., Papadakis, G.Z., et al., 2016. (68)Ga-DOTATATE for tumor localization in tumor-induced Osteomalacia. J. Clin. Endocrinol. Metab. 101 (10), 3575–3581.

Florenzano, P., Gafni, R.I., Collins, M.T., 2017. Tumor-induced osteomalacia. Bone Rep. 7, 90–97.

Fogelman, I., McKillop, J.H., Bessent, R.G., et al., 1978. The role of bone scanning in osteomalacia. J. Nucl. Med. 19 (3), 245–248.

Folpe, A.L., Fanburg-Smith, J.C., Billings, S.D., et al., 2004. Most osteomalacia-associated mesenchymal tumors are a single histopathologic entity: an analysis of 32 cases and a comprehensive review of the literature. Am. J. Surg. Pathol. 28 (1), 1–30.

Garcia, C.A., Spencer, R.P., 2002. Bone and in-111 octreotide imaging in oncogenic osteomalacia: a case report. Clin. Nucl. Med. 27 (8), 582–583.

Halperin, F., Anderson, R.J., Mulder, J.E., 2007. Tumor-induced osteomalacia: the importance of measuring serum phosphorus levels. Nat. Clin. Pract. Endocrinol. Metab. 3 (10), 721–725.

Ho, C.L., 2015. Ga68-DOTA peptide PET/CT to detect occult mesenchymal tumor-inducing osteomalacia: a case series of three patients. Nucl. Med. Mol. Imaging 49 (3), 231–236.

Ho, L.Y., Wong, P.N., Sin, H.K., et al., 2017. Risk factors and clinical course of hungry bone syndrome after total parathyroidectomy in dialysis patients with secondary hyperparathyroidism. BMC Nephrol. 18 (1), 12.

Hofman, M.S., Lau, W.F., Hicks, R.J., 2015. Somatostatin receptor imaging with 68Ga DOTATATE PET/CT: clinical utility, normal patterns, pearls, and pitfalls in interpretation. Radiographics 35 (2), 500–516.

Houang, M., Clarkson, A., Sioson, L., et al., 2013. Phosphaturic mesenchymal tumors show positive staining for somatostatin receptor 2A (SSTR2A). Hum. Pathol. 44 (12), 2711–2718.

Insogna, K.L., Briot, K., Imel, E.A., et al., 2018. A randomized, double-blind, placebo-controlled, phase 3 trial evaluating the efficacy of burosumab, an anti-FGF23 antibody, in adults with X-linked hypophosphatemia: week 24 primary analysis. J. Bone Miner. Res. 33 (8), 1383–1393.

Jadhav, S., Kasaliwal, R., Lele, V., et al., 2014. Functional imaging in primary tumour-induced osteomalacia: relative performance of FDG PET/CT vs somatostatin receptor-based functional scans: a series of nine patients. Clin. Endocrinol. 81 (1), 31–37.

Jain, N., Reilly, R.F., 2017. Hungry bone syndrome. Curr. Opin. Nephrol. Hypertens. 26 (4), 250–255.

Jiang, Y., Xia, W.B., Xing, X.P., et al., 2012. Tumor-induced osteomalacia: an important cause of adult-onset hypophosphatemic osteomalacia in China: report of 39 cases and review of the literature. J. Bone Miner. Res. 27 (9), 1967–1975.

Karunakaran, P., Maharajan, C., Ramalingam, S., et al., 2018. Is hungry bone syndrome a cause of postoperative hypocalcemia after total thyroidectomy in thyrotoxicosis? A prospective study with bone mineral density correlation. Surgery 163 (2), 367–372.

Kaya, C., Tam, A.A., Dirikoc, A., et al., 2016. Hypocalcemia development in patients operated for primary hyperparathyroidism: can it be predicted preoperatively? Arch. Endocrinol. Metab. 60 (5), 465–471.

Lamb, Y.N., 2018. Burosumab: First Global Approval. Drugs 78 (6), 707–714.

Ledford, C.K., Zelenski, N.A., Cardona, D.M., et al., 2013. The phosphaturic mesenchymal tumor: why is definitive diagnosis and curative surgery often delayed? Clin. Orthop. Relat. Res. 471 (11), 3618–3625.

Lee, H.K., Sung, W.W., Solodnik, P., et al., 1995. Bone scan in tumor-induced osteomalacia. J. Nucl. Med. 36 (2), 247–249.

Leow, M.K., Hamijoyo, L., Liew, H., et al., 2014. Oncogenic osteomalacia presenting as a crippling illness in a young man. Lancet 384 (9949), 1236.

Lewiecki, E.M., Urig Jr., E.J., Williams Jr., R.C., 2008. Tumor-induced osteomalacia: lessons learned. Arthritis Rheum. 58 (3), 773–777.

Li, D.M., Wu, H.W., Li, J.D., et al., 2018. Clinical and immunohistopathologic study of phosphaturic mesenchymal tumor. Zhonghua Bing Li Xue Za Zhi 47 (6), 427–431.
Minisola, S., Peacock, M., Fukumoto, S., et al., 2017. Tumour-induced osteomalacia. Nat. Rev. Dis. Primers 3, 17044.
Rai, G.S., Webster, S.G., Wraight, E.P., 1981. Isotopic scanning of bone in the diagnosis of osteomalacia. J. Am. Geriatr. Soc. 29 (1), 45–48.
Rayamajhi, S.J., Yeh, R., Wong, T., et al., 2019. Tumor-induced osteomalacia - current imaging modalities and a systematic approach for tumor localization. Clin. Imaging 56, 114–123.
Rendina, D., De Filippo, G., Tauchmanova, L., et al., 2009. Bone turnover and the osteoprotegerin-RANKL pathway in tumor-induced osteomalacia: a longitudinal study of five cases. Calcif. Tissue Int. 85 (4), 293–300.
Reubi, J.C., Schar, J.C., Waser, B., et al., 2000. Affinity profiles for human somatostatin receptor subtypes SST1-SST5 of somatostatin radiotracers selected for scintigraphic and radiotherapeutic use. Eur. J. Nucl. Med. 27 (3), 273–282.
Shastry, M., Kayani, I., Wild, D., et al., 2010. Distribution pattern of 68Ga-DOTATATE in disease-free patients. Nucl. Med. Commun. 31 (12), 1025–1032.
Sood, A., Agarwal, K., Shukla, J., et al., 2013. Bone scintigraphic patterns in patients of tumor induced osteomalacia. Indian J. Nucl. Med. 28 (3), 173–175.
Sun, Z.J., Jin, J., Qiu, G.X., et al., 2015. Surgical treatment of tumor-induced osteomalacia: a retrospective review of 40 cases with extremity tumors. BMC Musculoskelet. Disord. 16, 43.
Teasell, R.W., Shapiro, A.P., 2002. Misdiagnosis of conversion disorders. Am. J. Phys. Med. Rehabil. 81 (3), 236–240.
van der Rest, C., Cavalier, E., Kaux, J.F., et al., 2011. Tumor-induced osteomalacia: the tumor may stay hidden!. Clin. Biochem. 44 (14–15), 1264–1266.
Wang, L., Zhang, S., Jing, H., et al., 2018. The findings on bone scintigraphy in patients with suspected tumor-induced osteomalacia should not be overlooked. Clin. Nucl. Med. 43 (4), 239–245.
Witteveen, J.E., van Thiel, S., Romijn, J.A., et al., 2013. Hungry bone syndrome: still a challenge in the post-operative management of primary hyperparathyroidism: a systematic review of the literature. Eur. J. Endocrinol. 168 (3), R45–R53.
Yin, Z., Du, J., Yu, F., Xia, W., 2018. Tumor-induced osteomalacia. Osteoporos Sarcopenia 4 (4), 119–127.
Zhang, J., Zhu, Z., Zhong, D., et al., 2015. 68Ga DOTATATE PET/CT is an accurate imaging modality in the detection of culprit tumors causing osteomalacia. Clin. Nucl. Med. 40 (8), 642–646.